ARTICLES
https://doi.org/10.1038/s41566-021-00854-3
nature photonics



# Polaritonic nonlocality in light–matter interaction

Shima Rajabali[1]✉, Erika Cortese[2], Mattias Beck[1], Simone De Liberato[2]✉, Jérôme Faist[1] and Giacomo Scalari[1]✉

**Subwavelength electromagnetic field localization has been central to photonic research in the last decade, allowing us to enhance sensing capabilities as well as increase the coupling between photons and material excitations. The strong and ultrastrong light–matter coupling regime in the terahertz range using split-ring resonators coupled to magnetoplasmons has been widely investigated, achieving successive world records for the largest light–matter coupling ever achieved. Ever shrinking resonators have allowed us to approach the regime of few-electron strong coupling, in which single-dipole properties can be modified by the vacuum field. Here, we demonstrate, theoretically and experimentally, the existence of a limit to the possibility of arbitrarily increasing electromagnetic confinement in polaritonic systems. Strongly subwavelength fields can excite a continuum of high-momenta propagative magnetoplasmons. This leads to peculiar nonlocal polaritonic effects, as certain polaritonic features disappear and the system enters the regime of discrete-to-continuum strong coupling.**

Nanophotonic structures confine electromagnetic radiation below the Abbe diffraction limit by storing part of the electromagnetic energy into the kinetic energy of moving charges[1]. Primarily relying on metals as charge reservoirs, plasmonics has mainly targeted the visible portion of the electromagnetic spectrum. The possibility of extending plasmonic excitation to low frequencies (mid-infrared and terahertz)[2–4] by employing semiconductors and two-dimensional (2D) systems with plasma frequency tunable via the carrier concentration has allowed extreme electromagnetic field confinements in nanostructures[5]. In parallel, ultrastrong light–matter coupling[6,7] has recently drawn a great deal of attention due to the possibility of observing new quantum phenomena such as squeezed vacuum[8] and the long-sought superradiant quantum phase transition[9]. Several recent experiments have also allowed us to access and measure these squeezed states and their correlation properties[10,11]. Ultrastrong coupling (USC) takes place when the vacuum Rabi frequency ($\Omega_R$), measuring the resonant half-splitting between the lower (LP) and upper polariton (UP) branches, becomes a considerable fraction (customarily above 10%) of the frequency of the uncoupled systems ($\omega_0$). Semiconductor platforms allow a high degree of control and flexibility and have proven very successful for the study of this physics[8,12,13]. Multiple efforts have been made to scale down the size of photonic resonators[14–17]. This scaling aims to increase the light–matter coupling and reach the regime of few-electron strong coupling in molecular[18] and solid-state devices[19], where nonlinearities become important and individual electronic degrees of freedom can be manipulated[20,21].

Landau polaritons[22,23] are an experimental platform for light–matter coupling where magnetoplasmons—collective electronic excitations—play the role of matter (ultra)-strongly coupled to the near-field of electronic (*LC*) metamaterial photonic resonators. These have been demonstrated in electron and hole gases[24] confined in semiconductor heterostructures. The strongest achieved couplings ($\Omega_R/\omega_0 > 1.4$) make use of metallic split-ring resonators, which are able to confine the millimetre-wave radiation in extremely subwavelength volumes[25]. Reducing the capacitor gap in the *LC* circuit that constitutes the meta-atom has been shown to dramatically enhance the terahertz fields both for split-ring resonators[26] and non-resonant structures[27,28]. Obtaining the same field enhancement in cavities loaded with active material (that is, semiconductor quantum wells) nevertheless requires a careful analysis of the different components involved. An important question arises: what are the physical limitations to reducing the cavity volume and the subsequent increase of light–matter coupling? In this Article, we demonstrate how polaritonic nonlocal effects, consisting in the generation of high-momenta magnetoplasmons by the subwavelength resonator, effectively limit the achievable field confinement and thus the resonant polaritonic splitting. Our theory shows that discrete-to-discrete models underlying the polaritonic framework are no longer valid below a threshold gap size, as the increased momentum uncertainty due to spatial electromagnetic confinement couples the discrete cavity mode to a continuum of high-momenta magnetoplasmons. The system then converts to a discrete-to-continuum light–matter coupling model, whose non-perturbative physics has just recently begun to be investigated[29–32]. Experiments and finite-element simulations support this picture, demonstrating multiple novel nonlocal polaritonic features, as predicted by the theory. In particular, a reduction of the capacitor gap leads to a progressive disappearance of the UP branch and a vanishing contrast below a threshold magnetic field for the lower branch.

## Polaritonic nonlocality

Below critical length scales, the propagative nature of charge excitations in nanophotonic devices can no longer be neglected, leading to the emergence of nonlocal effects, as demonstrated in both plasmonic[33] and phononic[34] systems. In such a regime, the nanoscopic features confining the charge distribution, acting as a grating, allow the electromagnetic field to couple with high-momenta matter resonances. These modes can act as loss channels and reduce the field confinement by smearing the distribution of surface charges, thus ultimately limiting the achievable field enhancement.

In polaritonic systems, a different route towards nanoscopic confinement makes use of the electromagnetic field itself to define the coupled region out of an extended electronic system, as in metal nanogap resonators fabricated on top of a 2D electron gas (2DEG)[15]. Beyond the comparative ease of designing and tuning electromagnetic nanoresonators, this procedure also tends to maximize the

[1]Quantum Optoelectronics Group, Institute of Quantum Electronics, ETH Zürich, Zürich, Switzerland. [2]School of Physics and Astronomy, University of Southampton, Southampton, UK. ✉e-mail: shimar@phys.ethz.ch; s.de-liberato@soton.ac.uk; scalari@phys.ethz.ch

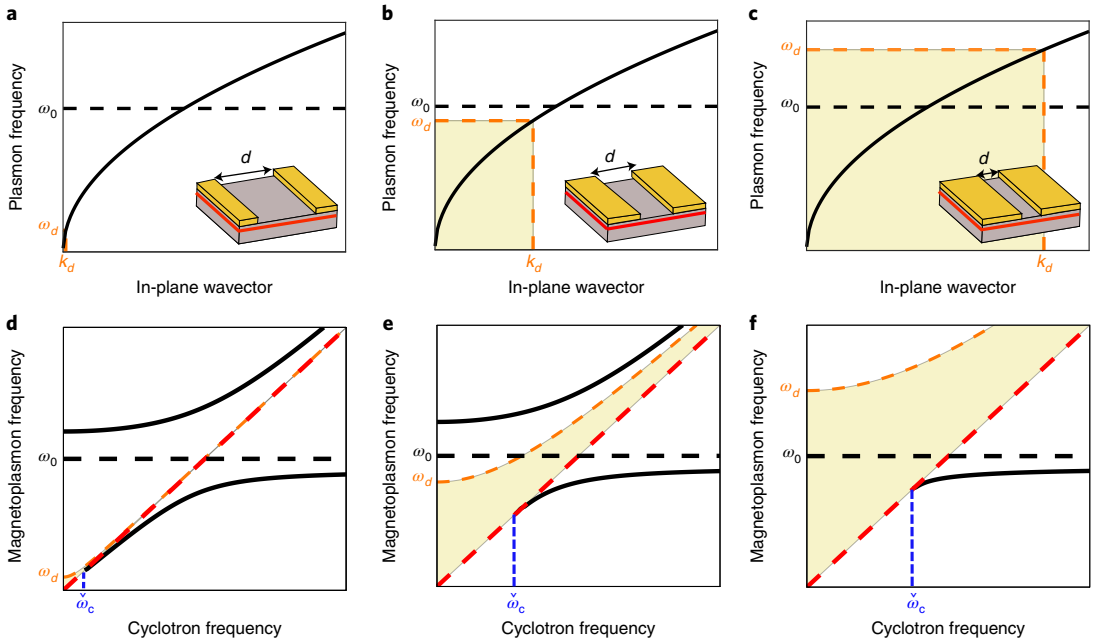


**Fig. 1 | Impact of nonlocality in nanoplasmonics. a–c**, Dispersion of the bare 2D plasma resonance as a function of the in-plane wavevector. A resonator with gap width $d$, as in the scheme shown in the inset, and a resonant frequency of $\omega_0$ (dashed black line) couples with plasma waves with in-plane wavevector up to value $k_d$, corresponding to the frequency range shaded in yellow, going from 0 to a maximal frequency $\omega_d$ at $B=0$. The gap width $d$ is decreasing from **a** to **c**. **d–f**, Polaritonic resonances, obtained from the coupling between the free plasmonic and photonic modes depicted in the top row, as a function of the cyclotron frequency. The yellow-shaded regions between the cyclotron transition $\omega_c$ (red dashed line) and the magnetically shifted edge of the continuum $\bar{\omega}_d = \sqrt{\omega_d^2 + \omega_c^2}$ (orange dashed line) highlight the continuum of possible magnetoplasmonic energies to which the photonic resonator (dashed black line) can couple. The LP merges into the continuum at the critical cyclotron frequency $\check{\omega}_c$. The position of the 2DEG is marked in red in the insets to **a–c**.

modal overlap between light and matter modes, and has contributed to multiple records in the achieved coupling strength[22,25,35,36]. In resonator-defined systems, nonlocal effects are also eventually bound to play a role. Tightly bound electromagnetic modes in fact have ill-defined momenta, making the standard momentum-space Hopfield approach inapplicable. In non-dispersive systems, strong light–matter coupling can still be studied using real-space approaches[37], but when the dispersion becomes non-negligible, we are obliged to take into account the coupling of the electromagnetic field to a continuum of high-momenta propagative electronic modes.

We have developed a polaritonic theory able to study nonlocal effects in an extended electronic system coupled to a photonic nanoresonator, allowing us to understand their impact on the precise engineering of light–matter coupling at the nanoscale. The optical response of a 2DEG in the absence of an applied magnetic field can be described in terms of 2D plasma waves indexed by their in-plane momenta $\mathbf{k}$. Their dispersion, shown in the top row of Fig. 1, is described by

$$\omega_P(k) = \sqrt{\frac{ke^2\rho_{2DEG}}{2m^*\varepsilon_0\varepsilon_r}}, \quad (1)$$

where $\rho_{2DEG}$ is the 2DEG density, $m^*$ the electron effective mass and $\epsilon_r$ the background effective dielectric function[38]. A perpendicular magnetic field $B$ with cyclotron frequency $\omega_c$ will dress the plasma waves, leading to field-dependent 2D magnetoplasmon resonances whose local non-retarded frequency is $\bar{\omega}_P(k) = \sqrt{\omega_P(k)^2 + \omega_c^2}$ (ref. [39]). Note that, in this Article, the bar over a frequency will be consistently used to indicate magnetically shifted frequency values.

The subwavelength nanoresonator breaks the in-plane translational invariance, and the in-plane wavevector $\mathbf{k}$ is thus not a conserved quantity in the light–matter interaction. The photon with frequency $\omega_0$ can thus couple with the continuum of plasma waves occupying the spectral region $\omega > \omega_c$. The strength of the interaction between the photon and plasma waves of frequency $\omega_P(k)$ is given by the coupling density $g(\omega_P(k))$, proportional to the 2D Fourier transform of the electromagnetic field profile in the 2DEG plane. If the smallest geometric feature of the electromagnetic field is of order $d$, its Fourier transform will have non-vanishing components up to a wavevector value $k_d$ of order $1/d$. The photon will thus couple with plasma waves having, for $B=0$, maximal frequency $\omega_d = \omega_P(k_d)$. This can be interpreted as a diffraction effect, in which the near-field of the photonic resonator diffracts in the far-field of the plasma waves.

The eigenequation of our system can be put in the form

$$\omega^2 - \omega_0^2 = \omega_0\left[\Delta(\omega) + i\Gamma(\omega)\right], \quad (2)$$

where $\Delta(\omega)$ and $\Gamma(\omega)$ are real functions whose expression can be found in the Methods. The function $\Gamma(\omega)$ is different from zero only in the region $\omega_c \leq \omega \leq \bar{\omega}_d$, shaded in the second row of Fig. 1. In this spectral interval, the frequency of the polaritonic resonances becomes complex, as the continuum of plasma waves irreversibly absorbs photons, even neglecting intrinsic plasmonic and photonic losses. The physics is akin to the one found in Landau damping[40], where in our case energy is dissipated generating plasma waves and not free electron–hole pairs.

Although, in a standard Landau polariton model[36], the two polaritonic branches exist for any value of the magnetic field, when $\omega_d$ becomes non-negligible the extreme photonic confinement can dramatically change the nature of the light–matter system as the narrow polaritonic resonances broaden and vanish into the continuum region. An analysis of the solutions of equation (2) shows the existence of a critical cyclotron frequency $\check{\omega}_c$ such that a narrow

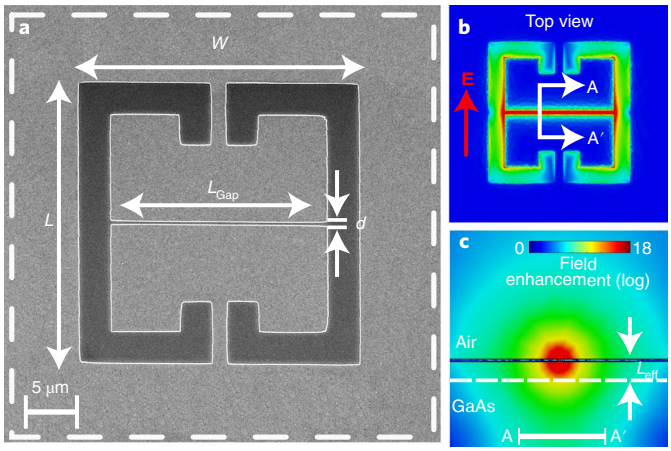


**Fig. 2 | Cavity and electric-field parameters. a**, SEM image of a unit cell (white dashed square) containing a cSRR with 250-nm gap, showing the resonator parameters, including gap size *d*. **b**,**c**, Cold-cavity electric-field distribution for the electric-field polarization direction perpendicular to the gap (red arrow), simulated by CST software for cSRRs resonating at 500 GHz, in two different views: top view (**b**) and the A–A′ view (or *y*–*z* plane) (**c**). $L_{eff}$ is defined in **c**. **b** and **c** share the same colour bar.

LP exists only for $\omega_c > \breve{\omega}_c$. A narrow UP instead exists if $\omega_0 > \bar{\omega}_d$, implying that the UP region is outside of the continuum, or if the coupling $g(\omega)$ is large enough to push the discrete resonance out of the continuum, analogously to the case studied in ref. [31] for the lower edge of the ionization continuum.

The physics described is sketched in Fig. 1. In Fig. 1a,d ($\omega_d, \breve{\omega}_c \approx 0$), the two polaritonic resonances are visible for most values of *B*, while in Fig. 1b,e ($\omega_d < \omega_0$) the UP is still present but the LP disappears for $\omega_c < \breve{\omega}_c$. For even smaller nanoresonators ($\omega_d > \omega_0$), the UP also disappears, as shown in Fig. 1c,f.

## Experimental results

We now proceed to the experimental study where we measure a 2DEG coupled to a metasurface of complementary split-ring resonators (cSRR)s in a series of samples where we vary the central gap width *d* from 4 μm down to 250 nm (the complete sample layout is shown in Supplementary Section 'Supporting experimental measurements' and Supplementary Fig. 1). A scanning electron microscopy (SEM) image of one unit cell of the metasurface is shown in Fig. 2a. The electric-field polarization direction used in the experiments to excite the *LC* mode of the resonator is perpendicular to the gap of the resonator (red arrow, Fig. 2b).

In the cold-cavity case (no 2DEG present), the electric field of the cSRR's fundamental mode is concentrated in the central gap for any value of gap *d* and its modal volume will scale as $V = L_{Gap} \times d \times L_{eff}$, where $L_{eff}$ is the effective penetration depth of the fringing field inside the substrate (Fig. 2c). Note that, as the central gap acts as a capacitor in the *LC* split-ring circuit, it directly affects the resonant frequency of the resonator, $\omega_0 = 2\pi f_{LC} = \frac{2\pi}{\sqrt{LC}}$. To allow for a meaningful comparison between different samples we thus rescaled the resonators to keep a fixed cSRR frequency at $f_{LC} = 500$ GHz.

Only the electrons within a cavity effective surface *S* of order $L_{Gap} \times d$ will couple to the strong transverse electric field of the resonator's *LC* mode, leading to a total effective electron number $N_{2DEG} = \rho_{2DEG} S$. The vacuum Rabi frequency $\Omega_R \propto \sqrt{\frac{N_{2DEG}}{V}}$, quantifying the resonant coupling of a discrete photonic mode to a single magnetoplasmon resonance, can then be explicitly written as

$$\Omega_R = \sqrt{\frac{e^2 \rho_{2DEG}}{4m^* \varepsilon_0 \varepsilon_r L_{eff}}}. \quad (3)$$

Although the explicit dependence of the coupling upon the gap width *d* cancels in equation (3), $L_{eff}$ changes due to the reduced *d* dimension. This dependency is borne out by our finite-element electromagnetic simulations for the cold-cavity case, where there is no 2DEG underneath the metallic surface, and showing a more confined and enhanced electric field in a narrower gap (Supplementary Section 'Supporting numerical simulations' and Supplementary Fig. 4). Reducing the gap size *d* is thus expected to increase the coupling $\Omega_R$ for a fixed cavity frequency[35].

The sample transmission is measured using terahertz time-domain spectroscopy at temperature $T = 2.7$ K as a function of an external out-of-plane magnetic field swept between 0 and 4 T. In the top row of Fig. 3a we report the experimental results. The colour map corresponding to a gap size of $d = 4$ μm ($\omega_0 \gg \omega_d$) shows an anticrossing of the first cavity mode with the linear cyclotron transition dispersion at an out-of-plane magnetic field $B \approx 1.2$ T. The solid black lines show the LP and UP branches fitted to the extracted maximum of transmission using our theory in the discrete-to-discrete regime, equivalent to the standard Hopfield model[22,36].

For the resonator with $d = 750$ nm ($\omega_0 > \omega_d$), we observe a broadening of the UP branch, but we can still extract the maximum of the transmission at each magnetic field. We plot the the normalized coupling ratio $\Omega_R/\omega_0$ extracted from a theoretical fit of the data for $d > 750$ nm, where the nonlocal effects discussed above are not relevant and the system is well described by a standard single-mode Hopfield model (Fig. 3b). In such a regime, we can extract a $\frac{1}{\sqrt{d}}$ dependence of the normalized coupling over the gap width (dashed brown line). For 500 nm ($\omega_0 \approx \omega_d$) and especially for 250 nm ($\omega_0 < \omega_d$) gap sizes, the upper branch no longer displays a clear maximum and the signal is broadened over a frequency range of over 200 GHz. Our optical measurements probe the photonic part of the polaritonic excitations, which, for the lower branch, naturally vanishes when $B \to 0$. This effect makes it difficult to highlight the LP disappearance at finite values of the magnetic field predicted by our theory. Inspection of Fig. 3a nevertheless shows a clear reduction of the lower branch visibility range for the smallest gap. It is worth noting that the slight changes in linewidth of the LP at its asymptotic limit are below the accuracy of our measurement set-up and do not have a physical interpretation.

To better compare to experimental results, Fig. 3a (bottom row) plots theoretical calculation results obtained including losses affecting both the photonic and magnetoplasmon fields. As detailed in the Methods, this has been accomplished by extending the dissipative diagonalization procedure for cavity quantum electrodynamics (CQED) from ref. [29]. The cyclotron transition $\omega_c$ (red dashed line) and the magnetically shifted continuum edge $\bar{\omega}_d = \sqrt{\omega_d^2 + \omega_c^2}$ (orange dashed line) bound the region of continuum magnetoplasmon energies shaded in Fig. 1, and they visualize the loss channel leading the broadening of the UP branch in our transmission data.

The enhanced transmission visible at higher frequencies in the experimental data is due to the second mode of the cSRRs lying close to 1 THz. This mode is not strongly confined in the gap and it is not relevant for the nonlocal physics of the system. It has thus not been included in the theoretical modelling. To clearly illustrate the UP broadening, sections of all four colour plots for both experimental and theoretical results in Fig. 3a, at zero magnetic field, are plotted in Fig. 3c,d. The progressive broadening of the UP branch is manifest. The clear blueshift of the UP from 4 μm to the 750-nm gap at zero magnetic field is related to the opening of the polariton gap[13], another indication of larger coupling strength in cSRRs with small slits[35].

The experimental transmission measurements also display linear dispersions appearing for the smallest gaps (indicated by black arrows in Fig. 3a). Such linear dispersions correspond to optical transitions at multiples of the cyclotron frequency.

In a 2DEG, the cyclotron resonance frequency should not depend on the carrier density, as the radiation couples only to the

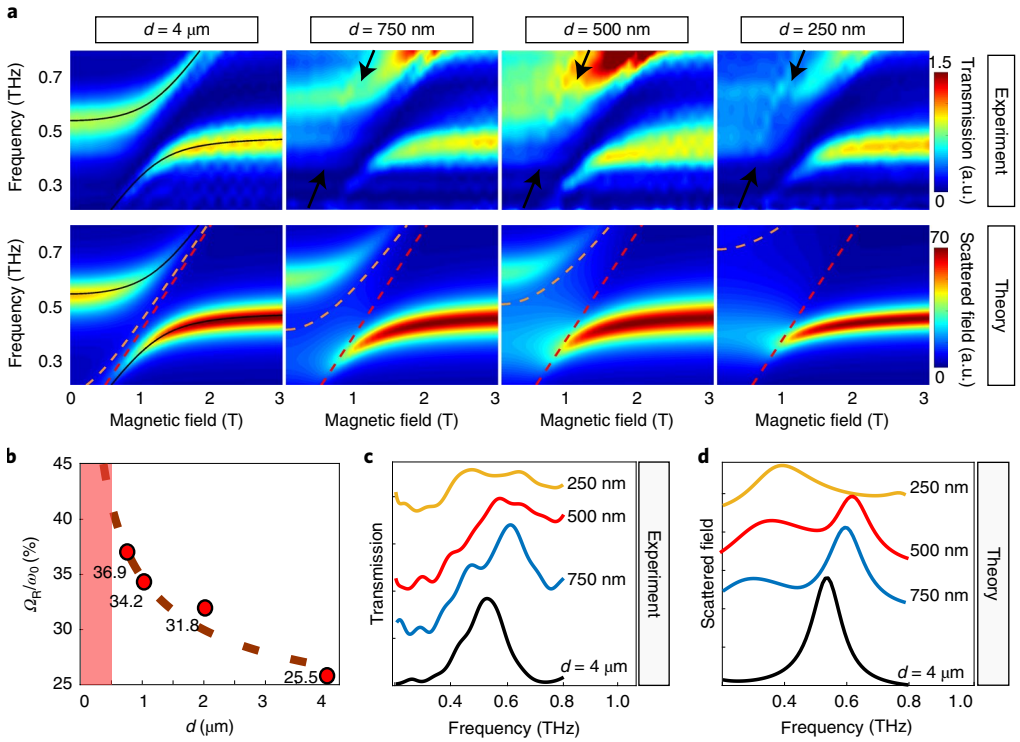


**Fig. 3 | Theory versus experiment. a**, Top row: transmission of cSRRs coupled to the Landau level transition in 2DEG versus magnetic field for four different gap sizes, *d*. Black arrows indicate an additional feature that corresponds to $f = 1.6 \times \omega_c/2\pi$, and the black solid lines are fitted LP and UP. Bottom row: the calculated scattered field for different gap feature sizes, *d* (same as the gap sizes of the experiment results). The regions between the cyclotron transition (red dashed line) and the magnetically shifted continuum edge (orange dashed line) are similar to the shaded regions on the bottom row of Fig. 1. **b**, Normalized coupling versus *d*. The dashed brown line indicates the predicted dependence of $\Omega/\omega$ on $\frac{1}{\sqrt{d}}$. The red-shaded region corresponds to where the large broadening of UP does not allow a measurement of the coupling. **c**,**d**, Sections (offset for clarity) of the colour plots in **a** at zero magnetic field for the experimental result (**c**) and the theoretical calculation (**d**).

centre-of-mass motion of the electron system. This very general result, known as Kohn's theorem[41], is strictly valid for parabolic bands and translationally invariant systems. Here, we observe a breaking of this theorem due to the presence of a spatially modulated charge density (the magnetoplasmon) that leads to a breaking of the translational invariance. The lack of translational invariance leads to a relaxation of the optical selection rules between Landau levels, allowing the observation of transitions at multiples of the cyclotron frequency. This effect has already been observed experimentally for the case of magnetoplasmons coupled to cyclotron resonance[38,42], but never in the context of Landau polaritons, where the momentum-matching element is part of an optical cavity. In this case, the observed effect is again arising due to the diffraction emerging with the introduction of very narrow resonator gaps.

## 3D finite-element electromagnetic simulations

To quantitatively confirm the theoretical predictions using the detailed cSRR geometry and visualize the nonlocal coupling to 2D magnetoplasmon modes, we turned to finite-element electromagnetic simulation (CST Microwave Studio) in which the 2DEG is modelled as a gyrotropic material. No 'effective medium' is adopted; that is, the dimensions of the different components, including the thickness of the quantum well layer (10 nm), are kept as in reality. The 2DEG electron density used in the simulation is calibrated by matching the cyclotron absorption strength with measurements performed on the bare (no cavity) heterostructure used in the experiment. A full description of the model and the employed parameters is provided in Supplementary Section 'Supporting numerical simulations' and Supplementary Fig. 5).

A set of simulations of the Landau polariton dispersion for a metallic metasurface with a gap of 250 nm, deposited on 2DEG, as a function of magnetic field is reported in Fig. 4a. In this simulation, the magnetic field is swept in the range $B \in [0, 4]$ T and can be compared directly with the corresponding experimental plot of Fig. 3a. The finite-element simulation is seen to reproduce very well the broadening of the UP branch. It is interesting to inspect the electric-field distribution at the anticrossing (white dashed line, Fig. 4a). As can be seen in Fig. 4d, the upper branch, expected to sit in the magnetoplasmon continuum, is completely dominated by the propagative plasmonic behaviour and the corresponding peak is largely broadened. Conversely, the lower branch (Fig. 4c) shows the electric-field intensity all concentrated in the gap. More simulation data for the broadening of the UP and partial disappearance of the LP are provided in Supplementary Section 'Supporting numerical simulations' and Supplementary Figs. 6–9).

## Conclusions

In summary, we have theoretically investigated the emergence of nonlocality in polaritonics. Contrary to nonlocality in plasmonic[33] and phononic[34] systems, which is caused by tight charge confinement, here nonlocal effects are driven by the confinement of the resonator's electromagnetic field coupling to a continuum of propagating magnetoplasma excitations. We experimentally observed such a physics using Landau polaritons at sub-terahertz frequencies by employing nanometre-sized resonators. First, we have shown that, when nonlocal effects are not relevant (gap size $d > 750$ nm), the normalized coupling ratio between light and matter scales as $\frac{1}{\sqrt{d}}$, increasing by ~50% from $d = 4$ μm to 750 nm, and reaching 37%

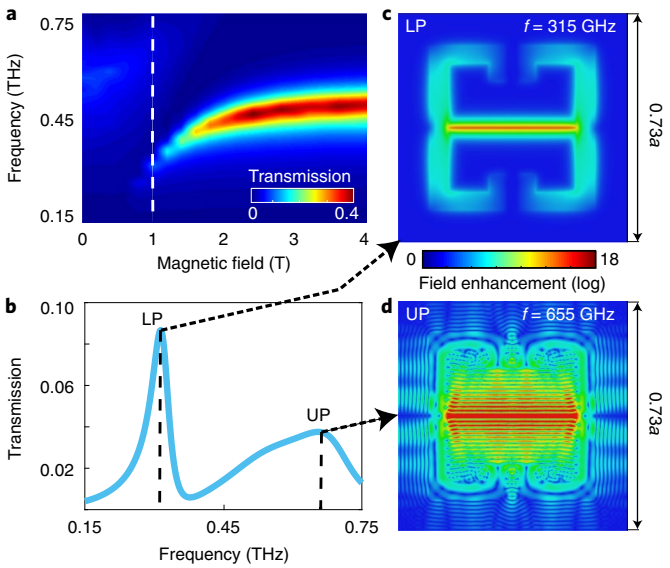


**Fig. 4 | Finite-element simulation for a cSRR with 250-nm gap on 2DEG.** **a**, Simulation of the Landau polariton dispersion as a function of magnetic field. **b**, The broadening and loss of contrast of the upper branch is evident in a section through the colour plot from **a** at anticrossing field $B = 1$ T. **c**,**d**, Electric-field distributions for the UP (**d**) and LP (**c**). The field distribution in **c** for the LP shows a pronounced electric-field concentration in the 250-nm gap and a corresponding narrow spectral distribution. On the other hand, **d** clearly demonstrates the excitation of plasmonic waves, and the corresponding peak in the frequency spectrum is broad. The unit cell size of the standard cSRR with $d = 4$ μm resonating at 500 GHz is $a = 50$ μm. The scaling factor for the resonator with $d = 250$ nm is 0.73.

for a single quantum well due to the strong field enhancement. For smaller gap values, nonlocal effects become dominant and the system is no longer well described by a standard Hopfield model. As predicted by our multimode dissipative bosonic Hamiltonian, we observe a broadening of the UP branch and partial disappearance on the lower one. Finite-element electromagnetic simulations confirm this interpretation. The presence of highly localized electric fields is also evidenced by the presence of features related to breaking of Kohn's theorem. Our findings set quantitative limits to the miniaturization of polaritonic devices and to the enhancement of polariton gaps, as well as opening new possibilities in the study of discrete-to-continuum strongly coupled systems[29,31,32].

The data that support the findings of this Article are available in the ETH Research Collection[43].

## Online content

Any methods, additional references, Nature Research reporting summaries, source data, extended data, supplementary information, acknowledgements, peer review information; details of author contributions and competing interests; and statements of data and code availability are available at https://doi.org/10.1038/s41566-021-00854-3.

Received: 7 January 2021; Accepted: 24 June 2021;
Published online: 9 August 2021

## References

1. Khurgin, J. et al. Landau damping and limit to field confinement and enhancement in plasmonic dimers. *ACS Photonics* **4**, 2871–2880 (2017).
2. Stanley, R. Plasmonics in the mid-infrared. *Nat. Photon.* **6**, 409–411 (2012).
3. Taliercio, T. & Biagioni, P. Semiconductor infrared plasmonics. *Nanophotonics* **8**, 949–990 (2019).
4. Zhang, X. et al. Terahertz surface plasmonic waves: a review. *Adv. Photon.* **2**, 014001 (2020).
5. Fei, Z. et al. Gate-tuning of graphene plasmons revealed by infrared nano-imaging. *Nature* **487**, 82–85 (2012).
6. Forn-Díaz, P. et al. Ultrastrong coupling regimes of light–matter interaction. *Rev. Mod. Phys.* **91**, 025005 (2019).
7. Frisk Kockum, A. et al. Ultrastrong coupling between light and matter. *Nat. Rev. Phys.* **1**, 19–40 (2019).
8. Ciuti, C., Bastard, G. & Carusotto, I. Quantum vacuum properties of the intersubband cavity polariton field. *Phys. Rev. B* **72**, 115303 (2005).
9. Nataf, P. & Ciuti, C. No-go theorem for superradiant quantum phase transitions in cavity QED and counter-example in circuit QED. *Nat. Commun.* **1**, 72 (2010).
10. Riek, C. et al. Direct sampling of electric-field vacuum fluctuations. *Science* **350**, 420–423 (2015).
11. Benea-Chelmus, I.-C. et al. Electric field correlation measurements on the electromagnetic vacuum state. *Nature* **568**, 202–206 (2019).
12. Anappara, A. A. et al. Signatures of the ultrastrong light–matter coupling regime. *Phys. Rev. B* **79**, 201303 (2009).
13. Todorov, Y. et al. Ultrastrong light–matter coupling regime with polariton dots. *Phys. Rev. Lett.* **105**, 196402 (2010).
14. Ballarini, D. & De Liberato, S. Polaritonics: from microcavities to sub-wavelength confinement. *Nanophotonics* **8**, 641–654 (2019).
15. Keller, J. et al. Few-electron ultrastrong light–matter coupling at 300 GHz with nanogap hybrid LC microcavities. *Nano Lett.* **17**, 7410–7415 (2017).
16. Jeannin, M. et al. Ultrastrong light–matter coupling in deeply subwavelength THz LC resonators. *ACS Photonics* **6**, 1207–1215 (2019).
17. Maissen, C. et al. Asymmetry in polariton dispersion as function of light and matter frequencies in the ultrastrong coupling regime. *New J. Phys.* **19**, 043022 (2017).
18. Chikkaraddy, R. et al. Single-molecule strong coupling at room temperature in plasmonic nanocavities. *Nature* **535**, 127–130 (2016).
19. Reithmaier, J. P. et al. Strong coupling in a single quantum dot-semiconductor microcavity system. *Nature* **432**, 197–200 (2004).
20. Todorov, Y. & Sirtori, C. Few-electron ultrastrong light–matter coupling in a quantum LC circuit. *Phys. Rev. X* **4**, 041031 (2014).
21. Ćwik, J. A. et al. Excitonic spectral features in strongly coupled organic polaritons. *Phys. Rev. A* **93**, 033840 (2016).
22. Scalari, G. et al. Ultrastrong coupling of the cyclotron transition of a 2D electron gas to a THz metamaterial. *Science* **335**, 1323–1326 (2012).
23. Paravicini-Bagliani, G. L. et al. Magneto-transport controlled by Landau polariton states. *Nat. Phys.* **15**, 186–190 (2019).
24. Keller, J. et al. Landau polaritons in highly nonparabolic two-dimensional gases in the ultrastrong coupling regime. *Phys. Rev. B* **101**, 075301 (2020).
25. Bayer, A. et al. Terahertz light–matter interaction beyond unity coupling strength. *Nano Lett.* **17**, 6340–6344 (2017).
26. Bagiante, S. et al. Giant electric field enhancement in split ring resonators featuring nanometer-sized gaps. *Sci. Rep.* **5**, 8051 (2015).
27. Chen, X. et al. Squeezing millimeter waves through a single, nanometer-wide, centimeter-long slit. *Sci. Rep.* **4**, 6722 (2014).
28. Bahk, Y.-M. et al. Ultimate terahertz field enhancement of single nanoslits. *Phys. Rev. B* **95**, 075424 (2017).
29. De Liberato, S. Virtual photons in the ground state of a dissipative system. *Nat. Commun.* **8**, 1465 (2017).
30. Forn-Díaz, P. et al. Ultrastrong coupling of a single artificial atom to an electromagnetic continuum in the nonperturbative regime. *Nat. Phys.* **13**, 39–43 (2017).
31. Cortese, E. et al. Strong coupling of ionizing transitions. *Optica* **6**, 354–361 (2019).
32. Cortese, E. et al. Excitons bound by photon exchange. *Nat. Phys* **17**, 31–35 (2021).
33. Ciracì, C. et al. Probing the ultimate limits of plasmonic enhancement. *Science* **337**, 1072–1074 (2012).
34. Gubbin, C. R. & De Liberato, S. Optical nonlocality in polar dielectrics. *Phys. Rev. X* **10**, 021027 (2020).
35. Maissen, C. et al. Ultrastrong coupling in the near field of complementary split-ring resonators. *Phys. Rev. B* **90**, 205309 (2014).
36. Hagenmüller, D., De Liberato, S. & Ciuti, C. Ultrastrong coupling between a cavity resonator and the cyclotron transition of a two-dimensional electron gas in the case of an integer filling factor. *Phys. Rev. B* **81**, 235303 (2010).
37. Gubbin, C. R., Maier, S. A. & De Liberato, S. Real-space Hopfield diagonalization of inhomogeneous dispersive media. *Phys. Rev. B* **94**, 205301 (2016).
38. Batke, E., Heitmann, D. & Tu, C. W. Plasmon and magnetoplasmon excitation in two-dimensional electron space-charge layers on GaAs. *Phys. Rev. B* **34**, 6951–6960 (1986).
39. Jin, D. et al. Topological magnetoplasmon. *Nat. Commun.* **7**, 13486 (2016).

40. Khurgin, J. B. Ultimate limit of field confinement by surface plasmon polaritons. *Faraday Discuss.* **178**, 109–122 (2015).
41. Kohn, W. Cyclotron resonance and de Haas–van Alphen oscillations of an interacting electron gas. *Phys. Rev.* **123**, 1242–1244 (1961).
42. Batke, E., Heitmann, D. & Kotthaus, J. P. Non-locality in the two-dimensional plasmon dispersion. *Phys. Rev. Lett.* **54**, 2367–2370 (1985).
43. Scalari, G. 2021. ETH Research Collection https://www.research-collection.ethz.ch/handle/20.500.11850/485912

## Methods

**Theoretical description of light–matter coupling.** We model the magnetoplasmonic excitations coupled to a single photonic mode using a generalization of the multimode Hamiltonian developed in ref. [31]

$$H = \hbar\tilde{\omega}_0 a^\dagger a + \sum_{\mathbf{k}} \hbar\bar{\omega}_P(k)\, b_{\mathbf{k}}^\dagger b_{\mathbf{k}} + i\hbar\Omega_R \sum_{\mathbf{k}} \sqrt{\frac{\bar{\omega}_P(k)}{\tilde{\omega}_0}} \left[a^\dagger + a\right]\left[\Xi_{\mathbf{k}} b_{\mathbf{k}} - \Xi_{\mathbf{k}}^* b_{\mathbf{k}}^\dagger\right], \tag{4}$$

where $a$ is the annihilation operator for a resonator photon and $b_{\mathbf{k}}$ annihilates a magnetoplasma wave with in-plane wavevector $\mathbf{k}=(k_x, k_y)$ and bare ($\omega_c=0$) frequency $\omega_P(k)$. The second-quantized operators obey bosonic commutation relations $\left[a, a^\dagger\right] = 1$ and $\left[b_{\mathbf{k}}, b_{\mathbf{k}}^{\dagger\prime}\right] = \delta_{\mathbf{k},\mathbf{k}'}$, where the $\delta$ is a Kronecker symbol. The Heisenberg equations generated by equation (4) are linear in the creation and annihilation operators, and such a quantum theory is thus equivalent to a semiclassical dielectric approach when the system is excited with classical light, as in our experiments. The quantum approach is nevertheless also able to model purely quantum results, when the polaritons are excited with non-classical light[44]. As better detailed in Supplementary Section 'Supporting theory', the photonic frequency $\tilde{\omega}_0$ includes the renormalization due to the diamagnetic $A^2$ term in the Hamiltonian, while $\bar{\omega}_P(k)$ is the magnetoplasmon frequency. In equation (4), the vacuum Rabi frequency $\Omega_R$ is given by equation (3) and $\Xi_{\mathbf{k}}$ is the 2D Fourier transform of the resonator field in the 2DEG plane. The explicit derivation of these quantities is provided in the Supplementary Information. Note that the Hamiltonian in equation (4) is not in the usual form found in polaritonic problems, where a dispersionless matter excitation (for example, transverse optical phonons in bulk) couples to a dispersive electromagnetic mode. In such a case, both light and matter have, in fact, the same spatial symmetry, and momentum conservation enforces a one-to-one coupling between light and matter modes. The model in equation (4) describes instead a one-to-many coupling, formally more similar to models used to describe losses in an open quantum system. In the continuum regime the Hamiltonian in equation (4) can be rewritten

$$H = \hbar\tilde{\omega}_0 a^\dagger a + \int_0^\infty \mathrm{d}\omega\, \hbar\bar{\omega}\, b(\omega)^\dagger b(\omega) + i\hbar\int_0^\infty \mathrm{d}\omega \sqrt{\frac{\bar{\omega}}{\tilde{\omega}_0}} \left[a^\dagger + a\right]\left[g(\omega) b(\omega) - g(\omega)^* b(\omega)^\dagger\right], \tag{5}$$

with $\left[b(\omega), b(\omega')^\dagger\right] = \delta(\omega-\omega')$, where the $\delta$ is now the Dirac function. The secular equation of the Hamiltonian in equation (5) is shown in equation (2), with

$$\Delta(\omega) = \frac{4\omega^2}{\omega_0} P\int_0^\infty \mathrm{d}\omega' \frac{|g(\omega')|^2}{\omega^2-\omega'^2-\omega_c^2}, \tag{6}$$

$$\Gamma(\omega) = \frac{2\pi\omega^2}{\omega_0} \frac{|g(\sqrt{\omega^2-\omega_c^2})|^2}{\sqrt{\omega^2-\omega_c^2}} \Theta(\omega-\omega_c), \tag{7}$$

where $P$ is the principal part and $\Theta(\omega)$ the Heaviside function. The minimal cyclotron frequency required for the existence of the LP $\breve{\omega}_c$ can be obtained by writing equation (2) for $\omega=\omega_c$, and solving for the critical value of the cyclotron frequency for which the LP merges into the continuum:

$$\breve{\omega}_c = \omega_0\left[1 + 4P\int_0^\infty \mathrm{d}\omega' \frac{|g(\omega')|^2}{\omega'^2}\right]^{-\frac{1}{2}}. \tag{8}$$

Analytical conditions for the existence of the UP could be determined analogously, although they are of limited interest being strongly dependent on the details of the specific resonator geometry. This asymmetry between the two polariton branches is due to the fact that the lower bound of the continuum, $\omega_c$, marks the existence of the plasma waves, while the upper bound, $\omega_d$, is more fuzzy, depending on the Fourier transform of the field profile, which does not necessarily present a well-defined sharp cutoff in $\mathbf{k}$ space.

**Theoretical description of the open system.** To better predict experimental features due to nonlocal nanopolaritonic effects, we need to consider the impact of intrinsic polariton losses due to the finite lifetime of both the cavity photon and the magnetoplasmon. With this aim we used the approach initially introduced by Huttner and Barnett to quantize the electromagnetic field in bulk dissipative dielectrics[45] and recently extended to the CQED case with both material and photonic losses[29]. This approach allows us to to write the system Hamiltonian in terms of a continuum of broadened photonic and magnetoplasmonic modes, with annihilation operators $A(\omega)$ and $B(\omega)$:

$$H_{\mathrm{tot}} = \int_0^\infty \hbar\omega A^\dagger(\omega)A(\omega) + \int_0^\infty \hbar\omega B^\dagger(\omega)B(\omega) + \hbar\int_0^\infty \mathrm{d}\omega \int_0^\infty \mathrm{d}\omega' \left[\zeta(\omega)A^\dagger(\omega) + \zeta^*(\omega)A(\omega)\right] \times \left[\theta(\omega')B^\dagger(\omega') + \theta^*(\omega')B(\omega')\right], \tag{9}$$

satisfying bosonic commutation relations $\left[A(\omega), A(\omega')^\dagger\right] = \left[B(\omega), B(\omega')^\dagger\right] = \delta(\omega-\omega')$. In the above Hamiltonian, the function $\zeta(\omega)$ contains the information about the photonic losses, and $\theta(\omega)$ contains a convolution integral between the resonant coupling density $g(\omega)$ and a function describing the frequency-dependent matter losses.

The Hamiltonian in equation (9) is then diagonalized by introducing operators for two orthogonal polariton branches $j=\pm$, obeying Bosonic commutation relations $\left[P_j(\omega), P_{j'}(\omega')\right] = \delta(\omega-\omega')\delta_{jj'}$, which we write in terms of the bare broadened fields:

$$P_j(\omega) = \int_0^\infty \mathrm{d}\omega' \left[x_j(\omega,\omega')A(\omega') + z_j(\omega,\omega')A^\dagger(\omega') + y_j(\omega,\omega')B(\omega') + w_j(\omega,\omega')B^\dagger(\omega')\right]. \tag{10}$$

The frequency-dependent Hopfield coefficients $(x_j, z_j, y_j, w_j)$ can then be found by solving the equations of motion $\omega P_j(\omega) = \frac{1}{\hbar}\left[P_j(\omega), H_{\mathrm{tot}}\right]$.

**As shown in ref.** [29], such a description is defined modulo a real function of $\omega$, fixing the basis used to specify the two degenerate modes $P_\pm(\omega)$. The two polaritonic operators are thus not individually identifiable with the two polaritonic branches, and the observable results have to be calculated from the gauge-invariant bare electromagnetic mode:

$$(a + a^\dagger) = \int_0^\infty \mathrm{d}\omega \sum_{j=\pm} M_j(\omega)\left[P_j(\omega) + P_j^\dagger(\omega)\right], \tag{11}$$

with $M_j$ being the electric component of the polaritonic field obtained by inverting the Hopfield transformation.

Numerical results are obtained by assuming that the only relevant scattering feature is across the $x$ axis, and it couples the photon resonator with plasma waves with wavevector up to the value $k_d = \frac{1}{d}$. We can then write $\Xi_{\mathbf{k}} = \Theta(k_d - |k_x|)\delta_{k_y,0}$, with $\Theta$ the Heaviside function, leading to a resonant coupling density of the form

$$g(\omega) = \Omega_R\sqrt{\frac{2\omega}{\pi\omega_d^2}}\Theta(\omega_d-\omega). \tag{12}$$

**Sample fabrication, measurement set-up and simulated structure in CST.** Information about sample fabrication, measurement set-up and the structure simulated in CST is available in Supplementary Sections 'Supporting experimental measurements' and 'Supporting numerical simulations'.

## Data availability

The numerical simulation and measurement data that support the plots within this paper are available from the corresponding author upon reasonable request. Data that support the findings of this Article are also available in the ETH Research Collection[43].

## Code availability

The codes used in the theory part of this study are available from the corresponding author upon reasonable request.

## References

44. López Carreño, J. C. et al. Exciting polaritons with quantum light. *Phys. Rev. Lett.* **115**, 196402 (2015).
45. Huttner, B. & Barnett, S. M. Quantization of the electromagnetic field in dielectrics. *Phys. Rev. A* **46**, 4306–4322 (1992).

## Acknowledgements

G.S., J.F. and S.R. thank J. Keller for help in the initial phase of the project. G.S. thanks M. Jeannin and R. Colombelli for discussions. S.R. thanks I.-C. Benea-Chelmus for fruitful discussions. G.S. and J.F. acknowledge financial support from ERC Advanced grant 'Quantum Metamaterials in the Ultra Strong Coupling Regime' (MUSiC) (ERC grant no. 340975). G.S. and J.F. also acknowledge financial support from the Swiss National Science Foundation (SNF) through the National Centre of Competence in Research Quantum Science and Technology (NCCR QSIT). S.D.L. is a Royal Society Research Fellow and was partly funded by the Philip Leverhulme Prize of the Leverhulme Trust. S.D.L. and E.C. acknowledge funding from the RGF\EA\181001 grant from the Royal Society.

## Author contributions

G.S., J.F. and S.D.L. conceived the idea. S.R. designed and fabricated the devices, carried out all the optical measurements, analysed all experimental data and performed numerical simulations under the supervision of G.S. and J.F. E.C. and S.D.L. developed the theory. E.C. performed numerical simulations under the supervision of S.D.L. M.B. performed the epitaxial growth. S.R., S.D.L. and G.S. wrote the manuscript. All authors discussed the results and commented on the manuscript.

## Competing interests
The authors declare no competing interests.

## Additional information
**Supplementary information** The online version contains supplementary material available at https://doi.org/10.1038/s41566-021-00854-3.

**Correspondence and requests for materials** should be addressed to S.R., S.D.L. or G.S.

**Peer review information** *Nature Photonics* thanks Angela Demetriadou, Antonio Fernandez-Dominguez, Jacob Khurgin and the other, anonymous, reviewer(s) for their contribution to the peer review of this work.